

APPLICATION AND COMPARATIVE ANALYSIS OF THE APES_CBI MODULE IN BEPC-II EXPERIMENTAL RESULTS

Siyuan Feng^{*1}, Zhiyuan Li¹, Zhe Duan, Weibin Liu¹,
Dou Wang, Na Wang¹, Yuan Zhang¹, Tianmu Xin,

Institute of High Energy Physics, Chinese Academy of Sciences, Beijing, China

¹also at University of Chinese Academy of Sciences, Beijing, China

Abstract

In this paper, we delve into the application and comparative analysis of the Accelerator Physics Emulation System Cavity-Beam Interaction (APES_CBI) module within the BEPC-II (Beijing Electron-Positron Collider) experiments. We developed the APES_CBI module as an advanced time-domain solver, specifically designed to analyze RLC circuits driven by beam and generator currents and to simulate the dynamic responses and synchrotron oscillations of charged particles within the cavity.

We begin by discussing our method for solving RLC parallel circuits, followed by an explanation of the logical architecture of our program. In the second part, we detailed our simulation results, starting with the BEPC-II electron ring. By comparing these results with experimental data, we validate the reliability of our simulations, showcasing our module's ability. Additionally, we extend our simulations to the CEPC Higgs mode on-axis injection conditions and studied the transient phase response to the sudden change of beam pattern.

INTRODUCTION

The growing complexity in particle accelerator design and simulation has significantly increased the demand for high-performance computational tools. To meet these challenges, particularly at the Circular Electron-Positron Collider (CEPC), we developed the 'APES' (Accelerator Physics Emulation System) software package. The APES_CBI module, originally developed to solve RLC circuits driven by beam and generator currents, is particularly adept at handling the dynamics of cavity-beam interaction. It effectively manages synchrotron oscillation and its impact on beam current patterns and charge distribution, offering insights into beam dynamics and improving predictive capabilities in collider experiments.

The paper is organized as follows: Section 2 introduces the solution method for RLC parallel circuits. Section 3 outlines the logical architecture of the APES_CBI program. Section 4 presents some of the simulation results obtained with APES_CBI. Section 5 discusses future development directions, including focusing on cavity interactions and Beam Loading effects to enhance simulation accuracy and efficiency.

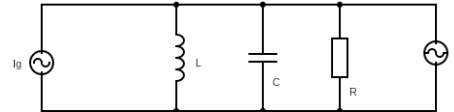


Figure 1: Parallel RLC circuit.

SOLVER OF RLC PARALLEL CIRCUIT

In the study of RF cavity circuit dynamics, we commonly model the interactions between the generator, beam, and cavity using a parallel RLC circuit. As illustrated in the Fig. 1, this circuit consists of a resistor R , a capacitor C , and an inductor L , which collectively respond to external excitations and internal feedback. This model not only aids in understanding the fundamental electrical behaviors within the RF cavity but also describes the mechanisms of energy storage and dissipation.

Following this, we will elaborate on the relationship between the generator current I_g and the cavity voltage V_{cav} , hereafter simply referred to as V , through a specific time-domain equation:

$$I_g(t) = \frac{V(t)}{R} + C \frac{dV(t)}{dt} + \frac{1}{L} \int_0^t V(\tau) d\tau. \quad (1)$$

In a simple example where the driving current is:

$$I_g(t) = u(0) \sin(\omega_{rf}t + \phi),$$

where ω_{rf} is the driving frequency of the amplifier, t is time, and ϕ is the phase of the drive. Applying the Laplace Transform to both sides, we obtain:

$$\hat{I}_g \frac{\omega_{rf} \times \cos(\phi) + s \times \sin(\phi)}{s^2 + \omega_{rf}^2} = \frac{\hat{V}}{R} + C(s\hat{V} - V(t=0)) + \frac{1}{L} \frac{\hat{V}}{s} \quad (2)$$

Now, let's consider a simple example where $V(t=0) = 0$, meaning we drive the circuit from zero stored energy. Plug this initial condition into equation(2) and move around the terms we will get:

$$\begin{aligned} \hat{V} &= \hat{I}_g \frac{\omega_{rf} \cos(\phi) + s \times \sin(\phi)}{s^2 + \omega_{rf}^2} \frac{1}{\left(\frac{1}{R} + Cs + \frac{1}{Ls}\right)} \\ &= \hat{I}_g \frac{s\omega_{rf} \cos(\phi) + s^2 \sin(\phi)}{C(s^2 + \omega_{rf}^2)(s^2 + \frac{1}{RC}s + \frac{1}{LC})} \\ &= \hat{I}_g \frac{s\omega_{rf} \cos(\phi) + s^2 \sin(\phi)}{C(s^2 + \omega_{rf}^2) \left[(s + \frac{1}{2RC})^2 + \frac{1}{LC} - \frac{1}{4R^2C^2} \right]} \end{aligned} \quad (3)$$

* fengsy@ihep.ac.cn

Redefine $\alpha = \frac{1}{2RC}$, and $\omega_0 = \sqrt{\frac{1}{LC} - \frac{1}{4R^2C^2}}$, we can do the inverse Laplace Transform, we will get the time domain expression of the Voltage, which has eight terms:

$$\begin{aligned}
V(t) = & \frac{\hat{I}_g}{C} \{ \omega_{rf} \cos(\phi) \times [\\
& \frac{e^{-j\omega_{rf}t}}{2[\alpha + j(\omega_0 - \omega_{rf})][\alpha - j(\omega_0 + \omega_{rf})]} + \\
& \frac{e^{j\omega_{rf}t}}{2[\alpha + j(\omega_0 + \omega_{rf})][\alpha - j(\omega_0 - \omega_{rf})]} + \\
& \frac{(\alpha + j\omega_0)e^{-\alpha t}e^{-j\omega_0 t}}{2j\omega_0 [\alpha + j(\omega_0 - \omega_{rf})][\alpha + j(\omega_0 + \omega_{rf})]} + \\
& \frac{-(\alpha - j\omega_0)e^{-\alpha t}e^{j\omega_0 t}}{2j\omega_0 [\alpha - j(\omega_0 + \omega_{rf})][\alpha - j(\omega_0 - \omega_{rf})]}] + \\
& \sin(\phi) \times [\\
& \frac{(-j\omega_{rf})e^{-j\omega_{rf}t}}{2[\alpha + j(\omega_0 - \omega_{rf})][\alpha - j(\omega_0 + \omega_{rf})]} + \\
& \frac{(j\omega_{rf})e^{j\omega_{rf}t}}{2[\alpha + j(\omega_0 + \omega_{rf})][\alpha - j(\omega_0 - \omega_{rf})]} + \\
& \frac{(\alpha + j\omega_0)^2 e^{-\alpha(t+t\phi)} e^{-j\omega_0(t+t\phi)}}{-2j\omega_0 [\alpha + j(\omega_0 - \omega_{rf})][\alpha + j(\omega_0 + \omega_{rf})]} + \\
& \frac{(\alpha - j\omega_0)^2 e^{-\alpha(t+t\phi)} e^{j\omega_0(t+t\phi)}}{2j\omega_0 [\alpha - j(\omega_0 + \omega_{rf})][\alpha - j(\omega_0 - \omega_{rf})]}] \}
\end{aligned} \tag{4}$$

Despite the complexity of these calculations, the results closely match our expectations.

PROGRAM STRUCTURE

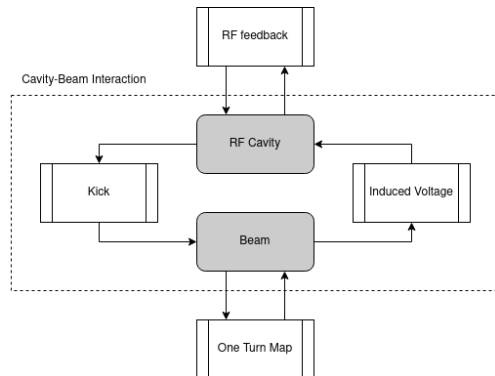


Figure 2: APES_CBI program structure. The dashed box indicates the interaction process between the beam and the cavity.

Figure 2 outlines the workflow of the APES_CBI module. As a particle arrives at the cavity, the generator voltage is computed based on the absolute arrival time of the particle using Equation 4. Subsequently, the additional voltage V_{add} generated as the particle passes through is calculated. The voltage seen by the particle, V_c , is the vector sum of the generator voltage, the beam voltage, and half of the voltage V_{add} it generates itself. The particle then receives a kick determined by V_c and the beam voltage V_{beam} is updated

with V_{add} for the computation of the next passing particle. Following this, a simple one-turn map calculation is employed using the slippage factor η to determine the absolute arrival time of the particle in the next turn.

SIMULATION RESULTS

Our simulations with the APES_CBI module covered the longitudinal tune shifts in BEPC-II's electron ring. By comparing our findings with both experimental data and theoretical predictions, we have confirmed our program's reliability. Furthermore, we utilized the module to simulate the on-axis injection process in the Higgs mode of CEPC.

Tune Shift in BEPC-II BER

We employ the APES_CBI module to benchmark the Beam Loading effects using existing data from the BEPC-II electron ring [1]. The parameters used for the simulation are listed in Table 1. The primary focus of this simulation is to investigate the longitudinal tune shifts.

Table 1: Main Parameters Relevant to the Machine Studies in BEPCII

Parameters, Unit	BER	BPR
Beam energy E , GeV	1.89	1.89
Circumference C , m	237.53	237.53
Momentum compaction α_p	0.017	0.017
Bunch number N_b	120	120
Synchrotron radiation U_0 , MV	0.12	0.12
RF frequency f_0 , MHz	499.8	499.8
R/Q of the RF cavity, Ω	47.65	47.65
RF voltage V_c , MV	1.60	1.51
Loaded quality factor Q	2.1×10^5	1.8×10^5
Synchrotron freq. f_s , kHz	37.96	36.82

The theoretical approach for calculating the tune shifts involves the following frequency domain formula given by Jiunn-Ming Wang [2]:

$$\Omega^2 - \omega_s^2 = i \frac{\alpha N_b I_b}{E/eT_0} \sum_{p=-\infty}^{\infty} (p N_b \omega_0 + \mu \omega_0 + \Omega) Z_{\parallel}(p N_b \omega_0 + \mu \omega_0 + \Omega) \quad (5)$$

Figure 3 depicts a comparison of the APES_CBI simulation results with the numerical solutions of the frequency domain formula and linear approximations. The simulation confirms the module's accuracy in simulating complex accelerator physics phenomena, particularly illustrating the impact of nonlinear effects in high current regions. Additionally, the simulation calculations were performed using the optimum detune, expressed as [3]:

$$\frac{\Delta\omega_{opt}}{\varrho} = \frac{I_{b,DC}F_b \cos(\phi)(R/Q)}{V} \quad (6)$$

where $\Delta\omega_{opt}$ represents the optimum detuning frequency, ω is the nominal frequency, $I_{b,DC}$ is the DC beam current, F_b is the bunch fill factor, ϕ is the synchronous phase angle, R/Q is the shunt impedance per unit charge, and V is the peak RF voltage.

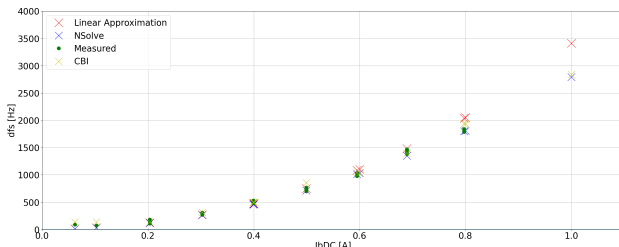


Figure 3: Comparison of APES_CBI simulation results with numerical and linear approximation solutions for tune shifts in the BEPC-II electron ring.

On-axis Injection Process in the CEPC Higgs Mode

During the on-axis injection process in the Higgs mode at CEPC, several bunches are transferred back to the booster ring from the storage ring and merged with the circulating smaller bunches. Initially, the number of merging bunches starts at seven and eventually increases to thirteen as the beam current in the booster ring decreases with the increasing number of bunches. To understand the dynamics under these conditions, we first analyze the synchrotron oscillations of the initial bunch.

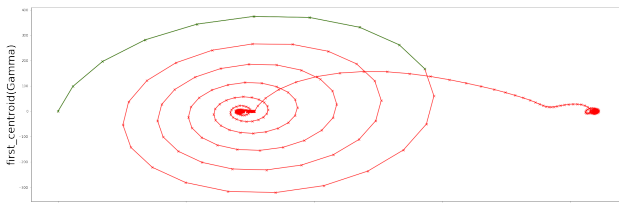


Figure 4: Synchrotron oscillation plot for the first bunch, showing changes in gamma over relative time.

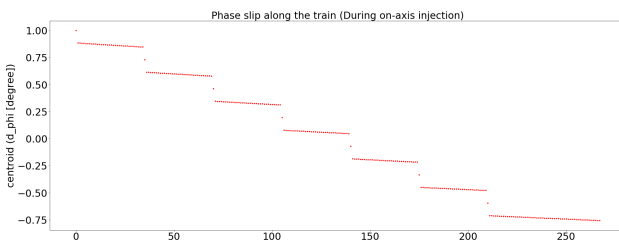


Figure 5: Phase slip plot along the bunch train after 1000 turns.

The synchrotron oscillation is depicted in Fig. 4, where the horizontal axis represents the relative time and the vertical axis depicts the changes in gamma. Following this analysis, we also examined the overall bunch distribution after 1,000 turns (shown in Fig. 5), which was significantly altered by the introduction of these large bunches.

CONCLUSION AND OUTLOOK

This paper has outlined our solutions for RLC parallel circuits, detailed the structure of the APES_CBI program, and discussed our findings from the Cavity-Beam Interaction (CBI) simulations at both BEPC-II and CEPC. By simulating BEPC-II's electron ring data, we confirmed the APES_CBI module's accuracy and efficiency in managing complex accelerator physics, particularly its capability to handle nonlinear effects in high current regions.

Looking forward, we are incorporating the CBI module into APES-T, an essential part of the APES project, which is a high-performance C/C++ simulation program, enables detailed particle tracking and accounts for nonlinear effects in complex accelerator lattices [4]. By integrating real-lattice tracking with beam-beam interactions and utilizing hybrid acceleration with GPU and MPI, APES-T aims to achieve more precise simulations. This integration is expected to develop a comprehensive accelerator simulation tool that includes a full lattice model and can compute beam-beam interactions, enhancing support for future accelerator design and research.

REFERENCES

- [1] N. Wang, Y. Zhang, C. Yu, G. Xu, and J. Dai, "Synchrotron tune shift due to the fundamental mode of the RF cavities", *Nucl. Instrum. Methods Phys. Res., Sect. A*, vol. 1014, p. 165725, Oct. 2021. doi:10.1016/j.nima.2021.165725
- [2] J.-M. Wang, "Modes of storage ring coherent instabilities", *AIP Conference Proceedings*, vol. 153, p. 697, 1987. doi:10.1063/1.36361.
- [3] Joachim Tückmantel, "Cavity-Beam-Transmitter Interaction Formula Collection with Derivation", Geneva, Switzerland, CERN-ATS-Note-2011-002, Oct. 2010.
- [4] Z. Li *et al.*, "Strong-strong beam-beam simulations with lattices of circular e+ e-colliders", *Nucl. Instr. and Meth. A*, vol 1064, p. 169386, 2024. doi:10.1016/j.nima.2024.169386